Eur. Phys. J. Special Topics **228**, 2023–2033 (2019)

https://doi.org/10.1140/epjst/e2019-800240-5

THE EUROPEAN PHYSICAL JOURNAL SPECIAL TOPICS

Regular Article

Chimera in a network of memristor-based Hopfield neural network

Fatemeh Parastesh[1], Sajad Jafari[1,a], Hamed Azarnoush[1], Boshra Hatef[2], Hamidreza Namazi[3], and Dawid Dudkowski[4]

[1] Department of Biomedical Engineering, Amirkabir University of Technology, 424 Hafez Ave., Tehran 15875-4413, Iran
[2] Neuroscience Research Center, Baqiyatallah University of Medical Sciences, Tehran, Iran
[3] School of Engineering, Monash University, Selangor, Malaysia
[4] Division of Dynamics, Lodz University of Technology, Stefanowskiego 1/15, 90-924 Lodz, Poland

Received 28 December 2018 / Received in final form 25 March 2019
Published online 14 October 2019

Abstract. Memristors have shown great potential to yield novel features in various domains. Therefore, memristor-based systems are being studied in widespread applications. In this paper, a newly proposed hyperbolic-type memristor-based Hopfield neural network is studied, as a single unit of a coupled network. Particularly, the effects of the coupling between each state variable of the system on the network behavior is investigated. It is observed that changing the coupling variable leads to different patterns at each coupling strength, including partial chimera state, chimera state, synchronization, imperfect synchronization and oscillation death. When the memristor-based elements are coupled with each other, increasing the coupling strength causes a regular transition from asynchronization to chimera state and then toward synchronization.

1 Introduction

Memristor is the fourth fundamental circuit element besides the resistor, the capacitor and the inductor, that was proposed by Leon Chua in 1971 [1]. Although many valuable properties were introduced for this new element, there was no useful model or example of memristor until 2008 [2,3]. In 2008, Hewlett-Packard laboratory found a solid-state thin film two-terminal memristor and just after that memristor attracted significant attentions [4–7]. Memristor is a passive two-terminal electronic device which describes a nonlinear relation between the charge (q) and the flux (φ) [8,9]:

$$d\varphi = M\,(q)\,dq. \tag{1}$$

A memristor with a non-constant M is a resistor with a memory [9] and when the applied voltage is turned off, it can remember the value of voltage [10]. Because of this property, it has been shown that memristor has similar features as the neural

[a] e-mail: sajadjafari@aut.ac.ir

synapse and can be used in artificial neural network [11,12]. The complex dynamics of the neurons are widely investigated in neuronal networks for various applications [13–15]. In biology, neurons communicate with each other in synapses and synaptic plasticity is the ability of weakening or strengthening of synapses during the time, in order to decrease or increase the activities. Therefore, synaptic plasticity is an important neurochemical foundation of storing the information and learning. Similar to biology, memristive-based neural networks can be used in machine learning and pattern recognition [16,17]. Thus for realizing brain functions, studying dynamics of a network of memristive neural network can be very effective and helpful.

In this paper, a network of hyperbolic-type memristor-based 3-neuron Hopfield neural network is studied [18] and its different behaviors is investigated, especially in search for chimera. Chimera state is a new phenomenon in nonlinear dynamics and has achieved lots of interests [19–23]. Chimera state emerges in an ensemble of identical coupled oscillators when both coherent and incoherent dynamics coexist [24]. It has been shown that chimera state is strongly related to neuronal systems and can be observed in various diseases including Parkinson's disease, epileptic seizures and brain tumors [25]. Chimera state is also associated with the real phenomena of uni-hemispheric slow-wave sleep in some birds and dolphins, in which half part of the brain is asleep and therefore the neurons are synchronized and the other half part is awake and its neurons are asynchronized [26]. Chimera state has been studied in various systems such as phased oscillators [27,28] and pendulum-like oscillators [29,30]. Recently, it has also been observed in different neuronal networks of either FitzHugh–Nagumo [31,32] model or Hindmarsh-Rose model [33–36].

Here we couple 100 memristor-based 3-neuron Hopfield neural networks non-locally and investigate the effects of changing the coupling variable. It is observed that the pattern is changed by varying the coupling variable at each coupling strength. Various states such as synchronization, chimera states, partial chimera state and oscillation death appear in the network in different coupling strengths. Partial chimera state is characterized by coexistence of incoherent and coherent regions when coherent region has a small width [37]. Simultaneous appearance of chimera, synchronization and oscillation death states in different coupling parameters and initial conditions, has been investigated in reference [38].

The remaining part of this paper is organized as follows: in the following section, the mathematical model of the memristor-based HNN and the coupled network is described. Section 3 investigates the effects of each variable in coupling and presents the resulting dynamics. Finally, conclusions are presented in Section 4.

2 Mathematical model of memristor-based HNN

A hyperbolic-type memristor-based Hopfield neural network is considered as a single unit of the network which was originally proposed by Bao et al. [18]. The connection topology for the system is shown in Figure 1.

According to Figure 1, the connection matrix can be as follows:

$$W = \begin{bmatrix} w_{11} & w_{21} & w_{31} \\ w_{12} & w_{22} & w_{32} \\ w_{13} & w_{23} & w_{33} \end{bmatrix} = \begin{bmatrix} -1.4 & 1.2 & -7 \\ 1.1 & 0 & 2.8 \\ kW & -2 & 4 \end{bmatrix}. \tag{2}$$

So the autonomous ordinary differential equations (ODEs) of the memristor-based HNN are described as:

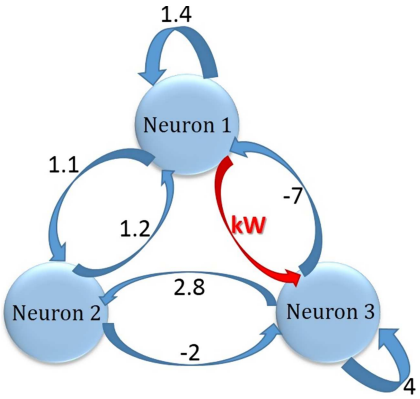

Fig. 1. Connection topology of memristor-based HNN [18].

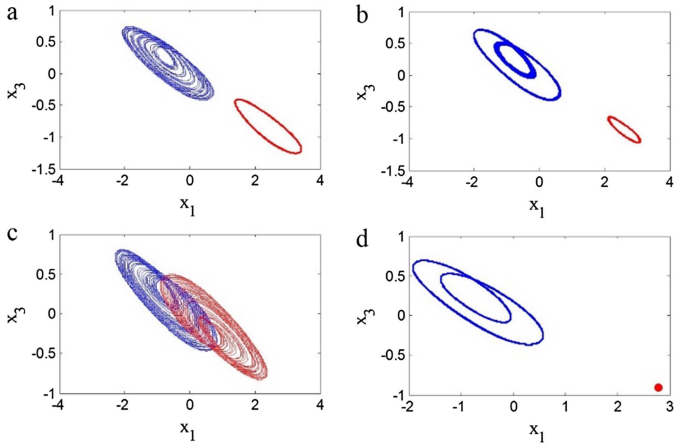

Fig. 2. Coexisting attractors of memristor-based HNN at $a = 1$: (a) coexistence of chaotic attractor and limit cycle at $b = 0.41$ and $k = 0.8$ with initial conditions at (0, 0.1, 0,0) and (−0.9, 0.1, 0.2, −0.7), (b) coexistence of two limit cycles at $b = 0.43$ and $k = 0.8$ with initial conditions at (0, ±0.1, 0,0), (c) coexistence of two strange attractors at $b = 0.01$ and $k = 0.95$ with initial conditions at (0, 0.1, 0,0) and (7.5, 0, −7.2, 0), and (d) coexistence of limit cycle and fixed point at $b = 0.46$ and $k = 0.8$ with initial conditions at (0, ±0.1, 0,0).

$$\begin{aligned}
\dot{x}_1 &= -x_1 - 1.4\tanh(x_1) + 1.2\tanh(x_2) - 7\tanh(x_3) \\
\dot{x}_2 &= -x_2 + 1.1\tanh(x_1) + 2.8\tanh(x_3) \\
\dot{x}_3 &= -x_3 + kW\tanh(x_1) - 2\tanh(x_2) + 4\tanh(x_3) \\
\dot{x}_4 &= -x_4 + \tanh(x_1)
\end{aligned} \tag{3}$$

where the synaptic weight w_{13} is defined as $kW = k(a - b\tanh(x_4))$ and k is the coupling strength of three neurons. By choosing different values for parameters of a, b and k, the system can exhibit different coexisting attractors of limit cycles and strange attractors, some of which are shown in Figure 2.

For our research, the network of abovementioned HNN is investigated. The equations of the network with coupling between all variables are given as follows:

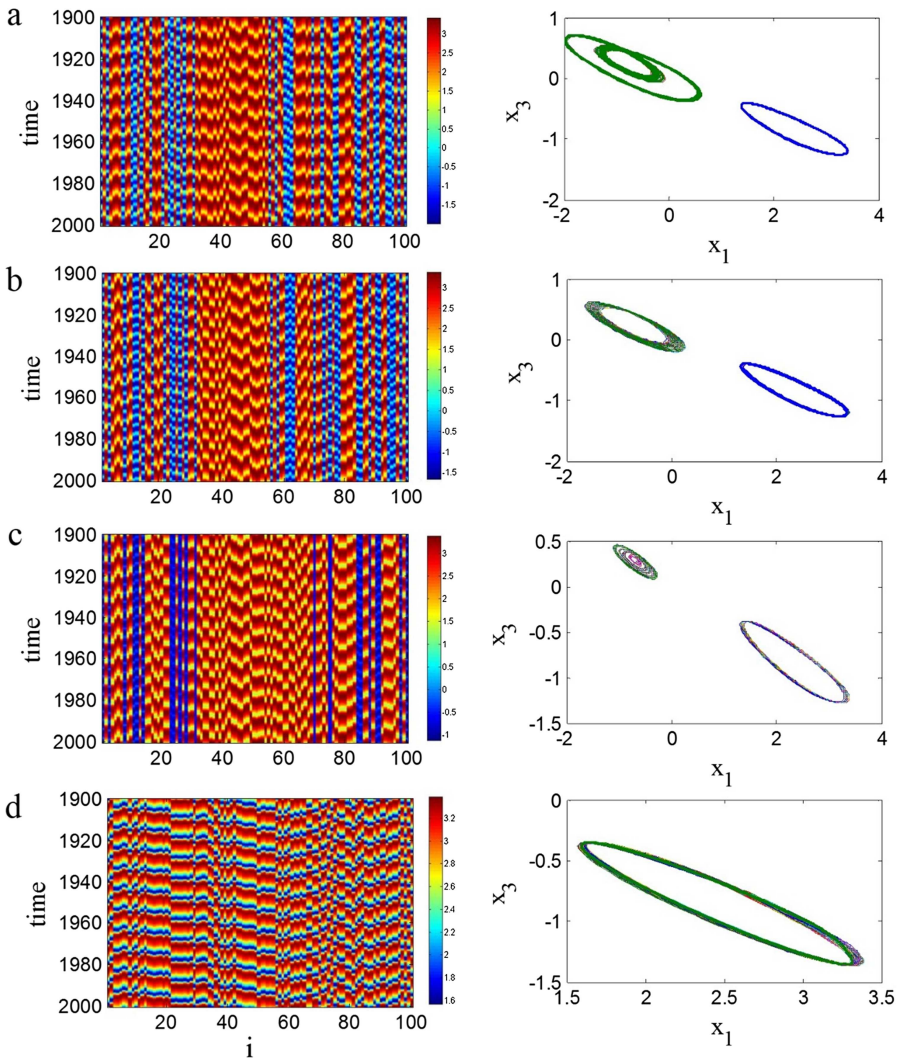

Fig. 3. Spatiotemporal patterns (left panel) and attractors of network (right panel) when coupling is between x_1 variables ($d_2 = d_3 = d_4 = 0$): (a) asynchronization for $d_1 = 0.01$, (b) asynchronization for $d_1 = 0.05$, (c) partial chimera state for $d_1 = 0.1$, and (d) partial chimera state for $d_1 = 0.5$.

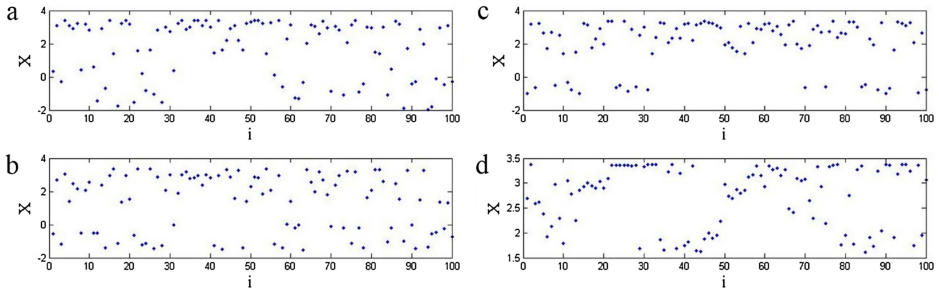

Fig. 4. The time snapshots of the X variables of the network corresponding to the Figure 3. (a) asynchronization for $d_1 = 0.01$, (b) asynchronization for $d_1 = 0.05$, (c) partial chimera state for $d_1 = 0.1$, and (d) partial chimera state for $d_1 = 0.5$.

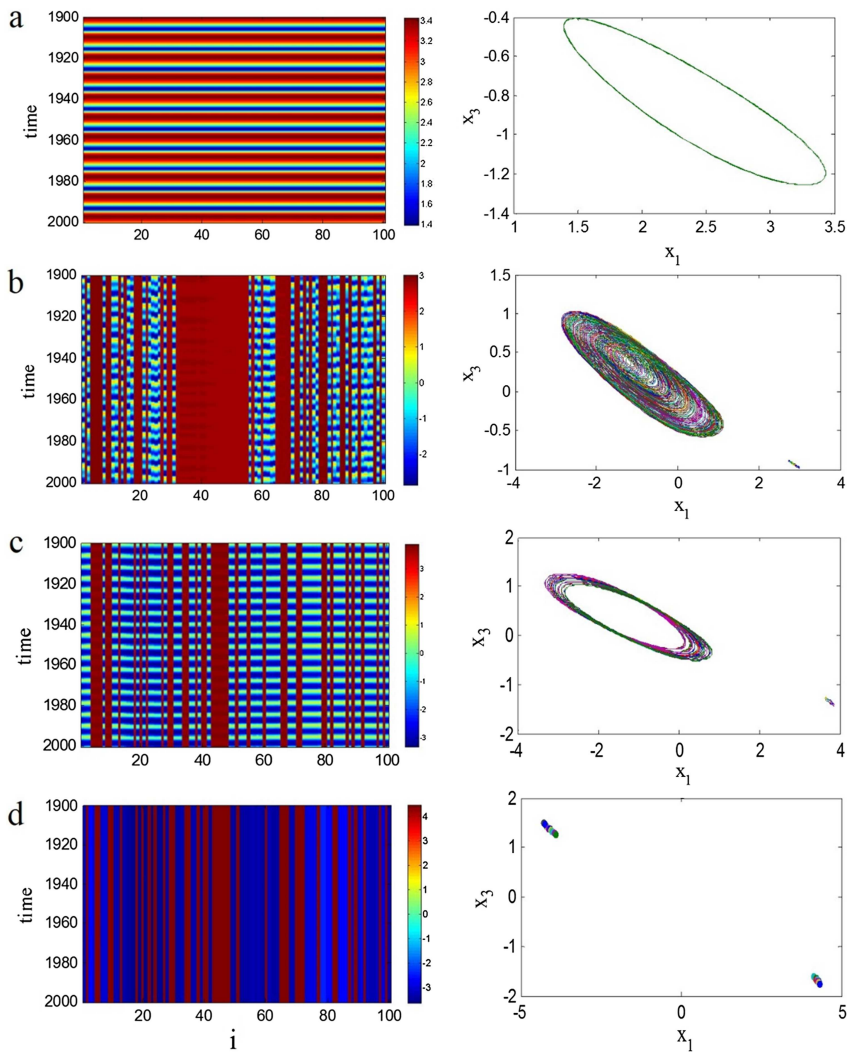

Fig. 5. Spatiotemporal patterns (left panel) and attractors of network (right panel) when coupling is between x_2 variables ($d_1 = d_3 = d_4 = 0$): (a) synchronization for $d_2 = 0.01$, (b) coexistence of coherent oscillation death and incoherent oscillations for $d_2 = 0.1$, (c) partial chimera state for $d_2 = 0.3$, and (d) incoherent oscillation death for $d_2 = 0.8$.

$$
\begin{aligned}
\dot{x}_{1i} &= -x_{1i} - 1.4\,\tanh(x_{1i}) + 1.2\,\tanh(x_{2i}) - 7\tanh(x_{3i}) + \frac{d_1}{2P}\sum_{j=i-P}^{i+P}[x_{1j} - x_{1i}] \\
\dot{x}_{2i} &= -x_{2i} - 1.1\,\tanh(x_{1i}) + 2.8\,\tanh(x_{3i}) + \frac{d_2}{2P}\sum_{j=i-P}^{i+P}[x_{2j} - x_{2i}] \\
\dot{x}_{3i} &= -x_{3i} + kW\,\tanh(x_{1i}) - 2\,\tanh(x_{3i}) + 4\,\tanh(x_{3i}) + \frac{d_3}{2P}\sum_{j=i-P}^{i+P}[c_{3j} - x_{3i}] \\
\dot{x}_{4i} &= x_{4i} + \tanh(x_{1i}) + \frac{d_4}{2P}\sum_{j=i-P}^{i+P}[c_{4j} - x_{4i}].
\end{aligned}
\tag{4}
$$

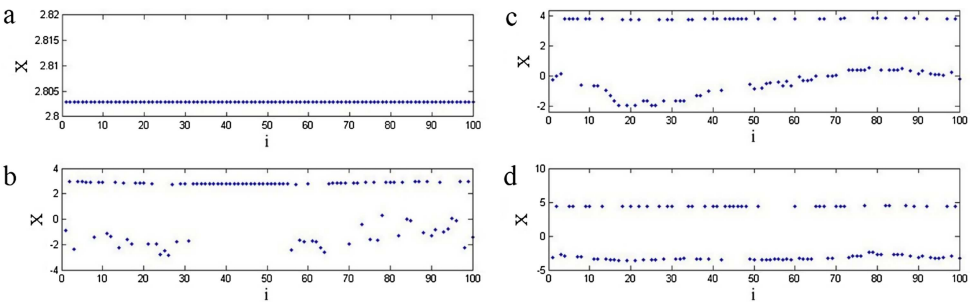

Fig. 6. The time snapshots of the X variables of the network corresponding to the Figure 5. (a) Synchronization for $d_2 = 0.01$, (b) coexistence of coherent oscillation death and incoherent oscillations for $d_2 = 0.1$, (c) partial chimera state for $d_2 = 0.3$, and (d) incoherent oscillation death for $d_2 = 0.8$.

Network (4) consists of N units and $[\dot{x}_{1i}, \dot{x}_{2i}, \dot{x}_{3i}, \dot{x}_{4i}]$ denote the state variables of ith unit. Each memristor-based HNN is symmetrically coupled to its $2P$ nearest neighbors and $d_1, \ldots, d_4$ denote the coupling strength values.

3 Results

The parameters of the systems are fixed as $a = 1$, $b = 0.41$ and $k = 0.8$. Thus each unit has coexistence of a limit cycle and a chaotic attractor as shown in Figure 2a. For constructing the network, $N = 100$ HNN are coupled and the value of P is set at $P = 30$. In all simulations, the initial conditions are chosen randomly from two basins of attraction.

3.1 x_1 state variable coupling

In the network of equation (4), the coupling is firstly set between x_1 state variables ($d_2 = d_3 = d_4 = 0$). Numerical simulations of the network (4), by increasing coupling strength d_1, are presented in Figure 3. When the coupling strength is small, the network dynamic is completely incoherent. However, some of initial conditions have been chosen from basin of chaotic attractor, but the coupling changes all the attractors to limit cycles. An example of this, is shown in Figure 3a for $d_1 = 0.01$. As the coupling strength becomes larger, a small number of oscillators become coherent and create partial chimera state, which is seen in Figures 3c and 3d. Furthermore, increasing the coupling strength changes the topology of the limit cycles. As can be seen in Figure 3d when $d_1 = 0.5$, all of the attractors become a unit limit cycle, but the oscillators are mostly spatially incoherent and the width of coherent oscillators is small. Figure 4 shows the corresponding time snapshots of the network in this case.

3.2 x_2 state variable coupling

Now the coupling is changed in a way that the couplings become between x_2 state variables instead of x_1 ($d_1 = d_3 = d_4 = 0$). Figure 5 shows the results of simulations for some coupling strength values d_2. For small values of coupling strength, the network is completely synchronous as shown in Figure 5a for $d_2 = 0.01$. When the coupling increases, some of the oscillators oscillate, whereas some others are attracted by fixed points. Figure 5b, shows the network pattern for $d_2 = 0.1$. In this case, a

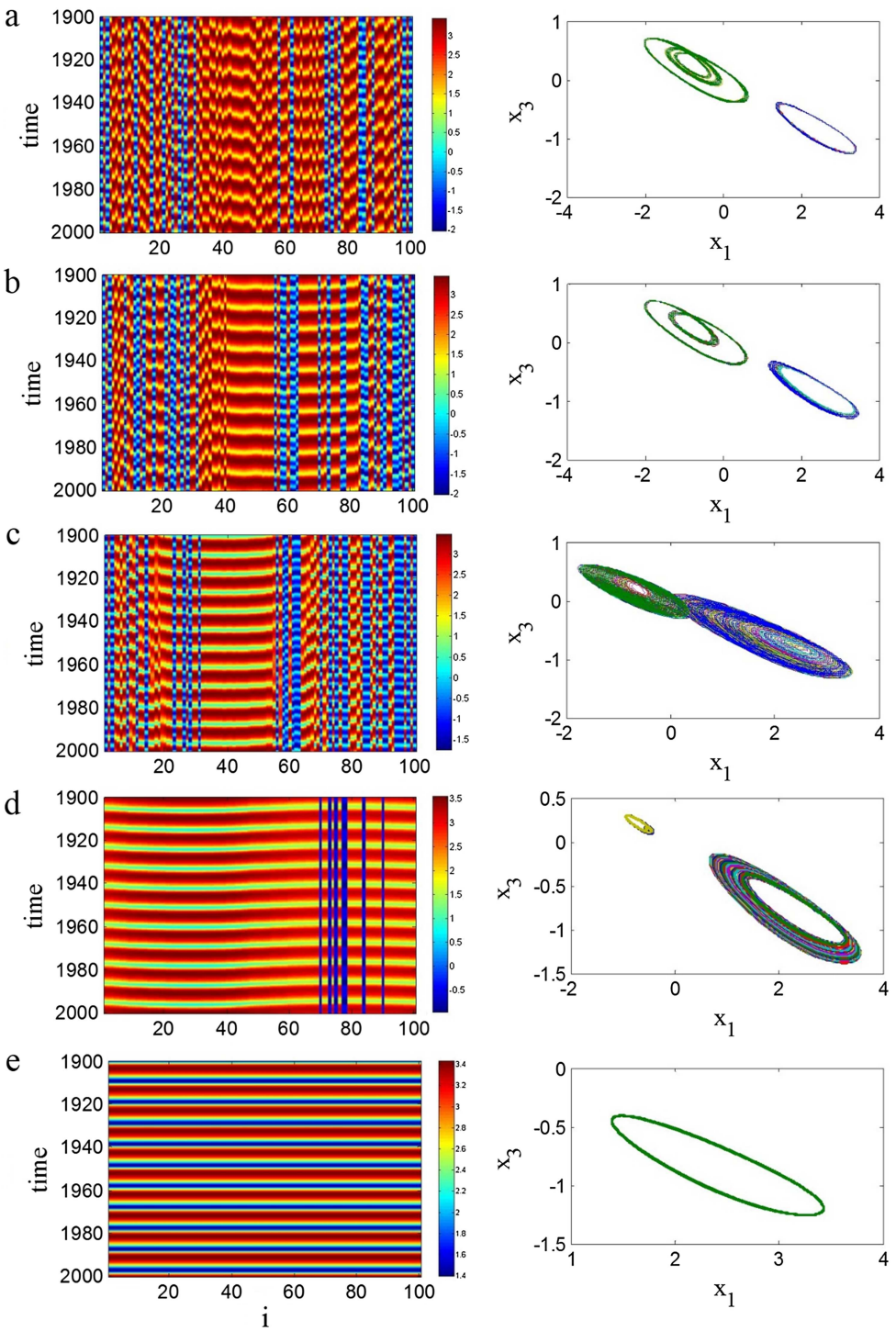

Fig. 7. Spatiotemporal patterns (left panel) and attractors of network (right panel) when coupling is between $x3$ variables ($d_1 = d_2 = d_4 = 0$): (a) asynchronization for $d_3 = 0.005$, (b) chimera state for $d_3 = 0.01$, (c) chimera state for $d_3 = 0.1$, (d) imperfect synchronization for $d_3 = 0.2$, and (e) synchronization for $d_3 = 0.3$.

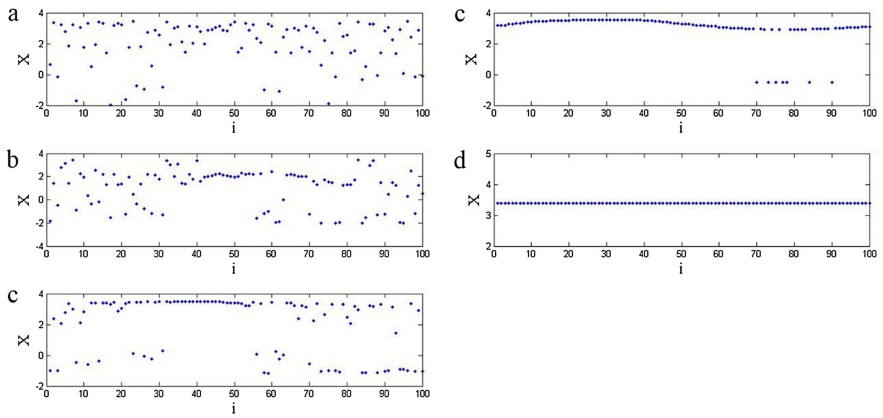

Fig. 8. The time snapshots of the X variables of the network corresponding to the Figure 7. (a) Asynchronization for $d_3 = 0.005$, (b) chimera state for $d_3 = 0.01$, (c) chimera state for $d_3 = 0.1$, (d) imperfect synchronization for $d_3 = 0.2$, and (e) synchronization for $d_3 = 0.3$.

large coherent oscillation death coexists with incoherent oscillators. If the coupling strength increases to $d_2 = 0.3$, partial chimera state appears, in which the coherent clusters have small widths (Fig. 5c). If we raise the coupling strength, all the oscillators will be attracted by fixed points and the pattern is incoherent oscillation death. Figure 5d shows this pattern for $d_2 = 0.8$. The time snapshots of this case are shown in Figure 6.

3.3 x_3 state variable coupling

In the next step the coupling is set between x_3 variables, which contains memristor terms ($d_1 = d_2 = d_4 = 0$). In this case, starting from very small coupling strength as shown in Figure 7a, the network is asynchronous. But by increasing coupling strength, chimera state emerges for a defined range of coupling which can be seen in Figures 7b and 7c) for $d_3 = 0.01$ and $d_3 = 0.1$, respectively. By further increasing of coupling strength, the network moves toward oscillating synchronously. At first the network exhibits imperfect synchronization as shown in Figure 7d and then by further increasing of d_3, synchronous state appears. Figure 8 shows the corresponding time snapshots of the patterns shown in Figure 7.

3.4 x_4 state variable coupling

Finally investigating the network is done by setting the coupling between x_4 variables ($d_1 = d_2 = d_3 = 0$). It was observed that the network is asynchronous for all the values of coupling strength d_4 and no synchronous or chimera state is emerged. Figure 9 shows the behavior network for some different coupling strengths when x_4 is the coupling variable. Figure 10 shows the corresponding time snapshots.

4 Conclusion

In this paper, synchronization patterns were studied in a network of hyperbolic-type memristor-based Hopfield neural network with non-local coupling. Memristors have

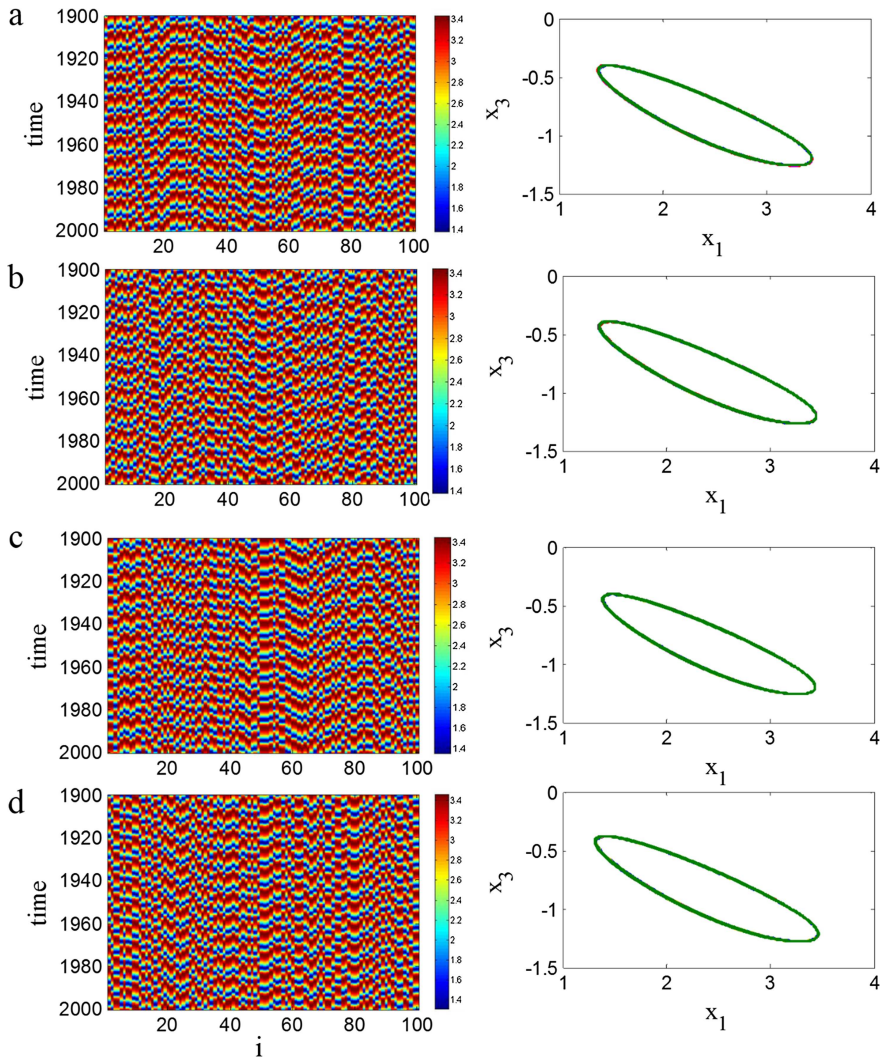

Fig. 9. Spatiotemporal patterns (left panel) and attractors of network (right panel) when coupling is between x_4 variables ($d_1 = d_2 = d_3 = 0$) for (a) $d_4 = 0.1$, (b) $d_4 = 0.3$, (c) $d_4 = 0.5$, and (d) $d_4 = 0.8$. The network is asynchronous for all values of d_4.

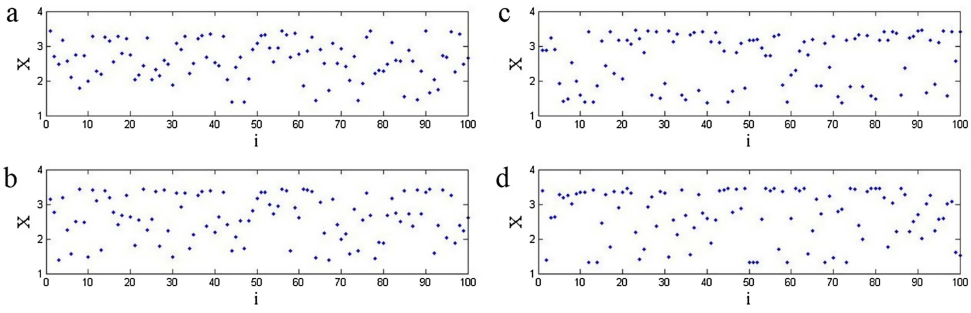

Fig. 10. The time snapshots of the X variables of the network corresponding to the Figure 9. (a) $d_4 = 0.1$, (b) $d_4 = 0.3$, (c) $d_4 = 0.5$, and (d) $d_4 = 0.8$. The network is asynchronous for all values of d_4.

special characteristics that are relevant to neurons. Thus memristor-based neural networks can be used for studying brain activities which have strong relations with synchronization and chimera states. The parameters of the system were chosen in a way that a single unit have coexistence of a limit cycle and a chaotic attractor. The network was investigated by varying the coupling strength and then by changing the coupling variable. The effects of the coupling range can be investigated in the future. It was observed that the network dynamics is strongly related to the coupling variable. Increasing the coupling strength leaded to different state transitions in each coupling variable. When x_1 variable was the coupling variable, asynchronization and partial chimera states appeared by increasing the coupling strength. When the coupling variable was changed to x_2, the network was synchronous for small coupling strength and by raising the coupling strength, the oscillators' attractors converted from limit cycles to fixed points. At first, coexistence of a coherent oscillation death region and incoherent oscillations was observed. Then the incoherent oscillations became coherent and finally at high coupling strengths, all the attractors were fixed points and an oscillation death state was observed. When the coupling variable changed to x_3, which contains the memristors, increasing the coupling strength caused transition from asynchronization to chimera state, and then to imperfect synchronization and finally complete synchronization. Subsequently, x_4 was selected as the coupling variable, but the network just exhibited asynchronous oscillations in this case.

Author contribution statement

All the authors designed research, performed research, and wrote the paper.

References

1. L. Chua, IEEE Trans. Circ. Theor. **18**, 507 (1971)
2. B. Bao, Z. Ma, J. Xu, Z. Liu, Q. Xu, Int. J. Bifurc. Chaos **21**, 2629 (2011)
3. D.B. Strukov, G.S. Snider, D.R. Stewart, R.S. Williams, Nature **453**, 80 (2008)
4. V.-T. Pham, C. Volos, S. Jafari, X. Wang, Optoelectron. Adv. Mater. Rapid Commun. **8**, 535 (2014)
5. K. Rajagopal, A. Bayani, A.J.M. Khalaf, H. Namazi, S. Jafari, V.-T. Pham, AEU Int. J. Electron. Commun. **95**, 207 (2018)
6. E. Tlelo-Cuautle, L.G. de la Fraga, V.-T. Pham, C. Volos, S. Jafari, A. de Jesus Quintas-Valles, Nonlinear Dyn. **89**, 1129 (2017)
7. Q. Xu, Y. Lin, B. Bao, M. Chen, Chaos Solitons Fractals **83**, 186 (2016)
8. B. Bo-Cheng, L. Zhong, X. Jian-Ping, Chin. Phys. B **19**, 030510 (2010)
9. C.K. Volos, I. Kyprianidis, I. Stouboulos, E. Tlelo-Cuautle, S. Vaidyanathan, J. Eng. Sci. Technol. Rev. **8**, 157 (2015)
10. S. Vaidyanathan, V.-T. Pham, C. Volos, in *Advances in memristors, memristive devices and systems* (Springer, 2017), p. 101
11. X. Li, R. Rakkiyappan, G. Velmurugan, Inf. Sci. **294**, 645 (2015)
12. V.-T. Pham, C. Volos, S. Jafari, X. Wang, S. Vaidyanathan, Optoelectron. Adv. Mater. Rapid Commun. **8**, 1157 (2014)
13. J. Ma, J. Tang, Sci. China Technol. Sci. **58**, 2038 (2015)
14. J. Ma, Y. Wu, H. Ying, Y. Jia, Chin. Sci. Bull. **56**, 151 (2011)
15. X. Song, C. Wang, J. Ma, J. Tang, Sci. China Technol. Sci. **58**, 1007 (2015)
16. C. Dias, J. Ventura, P. Aguiar, in *Advances in memristors, memristive devices and systems* (Springer, 2017), p. 305
17. R. Rakkiyappan, R. Sivasamy, X. Li, Circuits Syst. Sign. Process. **34**, 763 (2015)
18. B. Bao, H. Qian, Q. Xu, M. Chen, J. Wang, Y. Yu, Front. Comput. Neurosci. **11**, 81 (2017)

19. B.K. Bera, S. Majhi, D. Ghosh, M. Perc, EPL **118**, 10001 (2017)
20. D. Dudkowski, Y. Maistrenko, T. Kapitaniak, Phys. Rev. E **90**, 032920 (2014)
21. Z. Faghani, Z. Arab, F. Parastesh, S. Jafari, M. Perc, M. Slavinec, Chaos Solitons Fractals **114**, 306 (2018)
22. F. Parastesh, S. Jafari, H. Azarnoush, B. Hatef, A. Bountis, Chaos Solitons Fractals **110**, 203 (2018)
23. S. Rakshit, B.K. Bera, M. Perc, D. Ghosh, Sci. Rep. **7**, 2412 (2017)
24. A. Mishra, C. Hens, M. Bose, P.K. Roy, S.K. Dana, Phys. Rev. E **92**, 062920 (2015)
25. S. Majhi, M. Perc, D. Ghosh, Sci. Rep. **6**, 39033 (2016)
26. S. Majhi, B.K. Bera, D. Ghosh, M. Perc, Phys. Life Rev. (2018)
27. D.M. Abrams, S.H. Strogatz, Phys. Rev. Lett. **93**, 174102 (2004)
28. D. Dudkowski, Y. Maistrenko, T. Kapitaniak, Chaos **26**, 116306 (2016)
29. P. Jaros, Y. Maistrenko, T. Kapitaniak, Phys. Rev. E **91**, 022907 (2015)
30. T. Kapitaniak, P. Kuzma, J. Wojewoda, K. Czolczynski, Y. Maistrenko, Sci. Rep. **4** (2014)
31. I. Omelchenko, E. Omel'chenko, P. Hövel, E. Schöll, Phys. Rev. Lett. **110**, 224101 (2013)
32. I. Omelchenko, A. Provata, J. Hizanidis, E. Schöll, P. Hövel, Phys. Rev. E **91**, 022917 (2015)
33. B.K. Bera, D. Ghosh, M. Lakshmanan, Phys. Rev. E **93**, 012205 (2016)
34. S. Majhi, D. Ghosh, Chaos **28**, 083113 (2018)
35. S. Majhi, M. Perc, D. Ghosh, Chaos **27**, 073109 (2017)
36. Z. Wei, F. Parastesh, H. Azarnoush, S. Jafari, D. Ghosh, M. Perc, M. Slavinec, EPL **123**, 48003 (2018)
37. A. Gjurchinovski, E. Schöll, A. Zakharova, Phys. Rev. E **95**, 042218 (2017)
38. S. Majhi, P. Muruganandam, F. Ferreira, D. Ghosh, S.K. Dana, Chaos **28**, 081101 (2018)